Heterodyne mixing in diffusion-cooled superconducting aluminum hot-electron bolometers

I. Siddiqi,[a] A. Verevkin[b] and D. E. Prober
Department of Applied Physics, Yale University, 15 Prospect Street, New Haven, Connecticut 06520-8284

A. Skalare, W. R. McGrath, P. M. Echternach, and H. G. LeDuc
Center for Space Microelectronics Technology, Jet Propulsion Laboratory, Caltech, Pasadena, California 91109

(Received 12 July 2001; accepted for publication 18 December 2001)

We present microwave (30 GHz) measurements on aluminum superconducting hot-electron bolometer (HEB) mixers. Aluminum HEB mixers have a lower superconducting transition temperature than niobium and niobium nitride devices, and are predicted to have improved sensitivity and require less local oscillator power. The devices studied consist of a narrow superconducting aluminum microbridge with contacts comprised of thick aluminum, titanium, and gold. A perpendicular magnetic field is used to suppress superconductivity in the contacts. The device length is much shorter than the electron–phonon inelastic length $[L \ll (D\tau_{e-\mathrm{ph}})^{1/2}]$ and thus the intermediate frequency (IF) bandwidth is set by the diffusion time of hot electrons from the microbridge into the contacts. We discuss limitations on the IF bandwidth in very short HEB mixers with fully normal contacts. Overall, the microwave heterodyne mixing results show good performance with a mixer noise temperature inferred from the conversion efficiency and output noise of $T_M \geqslant 4$ K, double side band (DSB). Measurements at 618 GHz yield a conversion efficiency approximately 10 dB lower than observed at 30 GHz. Output saturation by background radiation is postulated to contribute significantly to this difference. A similar decrease in conversion efficiency in the microwave mixing measurements is observed when broadband noise is added to the rf input signal. We discuss the tradeoff between increased sensitivity and the occurrence of saturation effects in low transition temperature HEBs. © *2002 American Institute of Physics.*
[DOI: 10.1063/1.1448865]

I. INTRODUCTION

Over the past decade, considerable progress has been made in the field of terahertz heterodyne spectroscopy.[1–3] Many molecules that are involved in stellar formation and atmospheric chemistry undergo transitions between different rotational and vibrational states whose emission frequency is in the THz range.[4,5] For example, molecules such as H_2O, CO, and other light species are believed to be involved in the cooling of molecular gas clouds, an important step in star formation.[4,6] In the Earth's atmosphere, the OH^- radical plays a significant role in ozone chemistry, and can be detected by way of the doublet lines at 2.510 and 2.514 THz.[7] Several space-borne and ground based remote sensing missions are planned for near term deployment, and there is a need for heterodyne detectors with improved sensitivity that operate at THz frequencies.[8–10]

Nb/Al-AlO_x/Nb supercondcutor–insulator–superconductor (SIS) tunnel junction mixers exhibit near-quantum-noise-limited performance at operating frequencies of several hundred GHz. However, rf losses in the Nb superconducting tuning circuit limit the use of these detectors to frequencies near or below the superconducting energy gap frequency, ~700 GHz. Operation up to ~1.2 THz is achieved using NbTiN ($T_C \sim 14$ K) for the wiring layer.[11] Schottky diode mixers can be used at THz frequencies, but require more local oscillator (LO) power than SIS mixers (mW versus μW), and have considerably lower sensitivity. Schottky mixers recently developed for the earth observing system (EOS) Aura satellite have demonstrated a receiver noise temperature $T_R = 9000$ K, DSB at 2.5 THz (T_M is estimated to be 3500 K) with 5 mW of absorbed LO power.[7]

The superconducting hot-electron bolometer (HEB) mixer offers low noise operation at frequencies above 1 THz while requiring considerably less LO power than a Schottky mixer.[12] The device consists of a thin, narrow superconducting microbridge contacted with thick normal metal contact pads. High frequency radiation consisting of the rf signal to be detected and the LO are coupled to the HEB device using quasioptical or waveguide techniques.[13,14] The combination of LO and dc power puts the device into the operating state where the resistance of the superconducting HEB varies strongly with the electron temperature. The thermal response time (τ_{th}) is not so short that the electron temperature various at the LO or rf signal frequencies. However, if the intermediate frequency [(IF); $f_{\mathrm{IF}} = |f_{\mathrm{RF}} - f_{\mathrm{LO}}|$] is smaller than the thermal relaxation rate, then the resistance of the HEB is modulated at this intermediate frequency. The mixer conver-

[a]Electronic mail: irfan.siddiqi@yale.edu
[b]Current address: University of Rochester, 240 E. River Rd., Rochester NY, 14623.

sion efficiency is defined as the ratio of the power at the IF to the input rf power,

$$\eta(f_{\mathrm{IF}}) \equiv P_{\mathrm{IF}}/P_{\mathrm{RF}} = \eta(0)/[1+(2\pi f_{\mathrm{IF}}\tau_{\mathrm{th}})^2]. \quad (1)$$

The -3 dB IF bandwidth of the mixer is determined by the thermal relaxation rate

$$f_{\mathrm{IF},-3\mathrm{dB}} = 1/(2\pi\tau_{\mathrm{th}}). \quad (2)$$

In the presence of strong electrothermal feedback effects, the observed rolloff in the IF response is described by an effective time constant which is equal to the thermal time divided by $(1-\alpha)$. The parameter α can be predicted from the pumped current–voltage characteristic and is a measure of the strength of the electrothermal feedback between the electron temperature and the dc bias supply.[15] In our experiments, $\alpha \ll 1$, and Eq. (2) may be used.

There are two main mechanisms by which hot electrons are cooled in HEB mixers. Energy relaxation can occur through inelastic electron–phonon scattering, ultimately leading to heat being transferred via phonons into the substrate.[16] Alternatively, if the device length is shorter than the inelastic electron–phonon length ($L \ll L_{e-\mathrm{ph}}$), then the dominant mode of energy relaxation is outdiffusion of hot electrons from the superconducting microbridge into the contact pads.[17] This diffusion–cooling technique allows for ultrawide IF bandwidths to be achieved using materials where the electron–phonon inelastic scattering rate is too slow for practical detectors.

Thin film Nb ($T_C \sim 5-6$ K) phonon-cooled devices have an IF bandwidth of order 100 MHz.[16] This is too small for most applications. NbN ($T_C \sim 10$ K) has been shown to have an electron–phonon inelastic scattering time of 12 ps at 10 K, and hence devices with up to 10 GHz of bandwidth should be possible.[18] However, even for very thin NbN films, the phonon escape time is comparable to the electron–phonon time and hence both parameters need to be considered in mixer design. Typically, the film thickness and the acoustic transparency of the film–substrate interface are the parameters of interest. IF bandwidths of ~ 5 GHz have been attained using NbN films on MgO substrates.[19] Typical values of the receiver noise temperature are $T_R = 2900$ K, DSB at 2.5 THz.[20]

For diffusion-cooled devices, the IF bandwidth is determined by the diffusion time (τ_{diff}) of hot electrons from the microbridge to the contact pads. This can be shown to equal[21]

$$\tau_{\mathrm{th}} = \tau_{\mathrm{diff}} = L^2/(\pi^2 D), \quad (3)$$

where L is the microbridge length and D is the diffusion constant. An IF bandwidth of 9 GHz with a receiver noise temperature of $T_R = 1800$ K, DSB at 2.5 THz has been demonstrated with a Nb HEB with $L = 0.08$ μm. The absorbed LO power was estimated to be 30 nW.[22]

The motivation of the present work is to improve HEB performance by using Al ($T_C \sim 1-2$ K) for the microbridge. A HEB mixer with a critical temperature lower than Nb has been predicted to have lower mixer noise and to require less LO power.[23] The dominant source of noise in a well optimized HEB mixer is thermal fluctuation noise. Karasik and

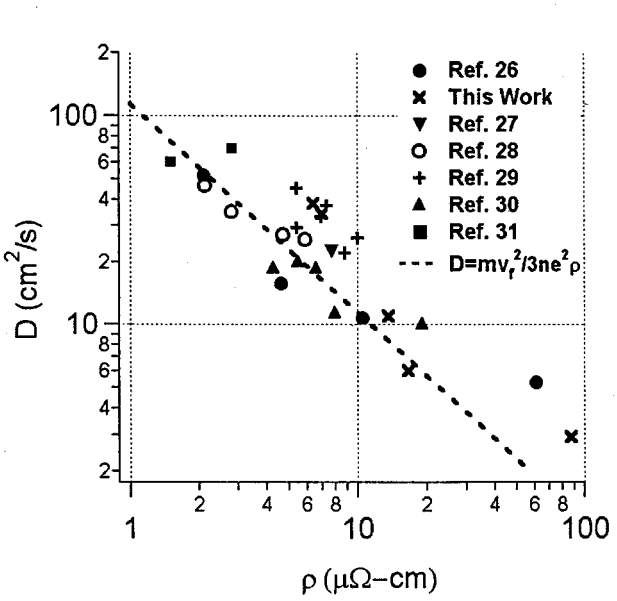

FIG. 1. Diffusivity vs resistivity for Al films with thickness 7–25 nm.

Elantiev[24] have calculated that the mixer noise temperature under ideal operating conditions is a few times the critical temperature. Prober[17] also predicts that the mixer noise should be proportional to T_C. It appears generally true that thermal fluctuations contribute to the mixer noise temperature proportional to T_C. Though a complete theory of noise in HEBs is still under development, we propose simply that an improvement in mixer noise should occur when the thermal noise components are reduced. The theories referenced above do not take quantum effects into account, and it is understood that HEB mixers have a lower bound on the noise temperature dictated by quantum mechanics ($T_M > h\nu/k$). However, current devices have not reached such quantum-limited sensitivity and thus lower T_C devices are predicted to have lower mixer noise temperatures.

The LO power required for mixing in a diffusion-cooled device[25] is given by

$$P_{\mathrm{LO}} = (4\mathfrak{L}/R)(T_C^2 - T^2), \quad (4)$$

where $\mathfrak{L} = 2.45\times 10^{-8}$ $W\text{-}\Omega/\mathrm{K}^2$ is the Lorenz constant, R is the device electrical resistance, and T is the temperature of the contact pads (the ''bath'' temperature). In typical operation $T \ll T_C$, so lowering T_C of the HEB should significantly reduce the required LO power. This is important for actual applications where the use of a solid state LO source is desired, or in array applications. For $T \ll T_C$, $P_{\mathrm{LO}} \propto T_C^2$.

An additional advantage of Al is that high diffusivity thin films can be readily prepared, and hence shorter diffusion times can be achieved. Shown in Fig. 1 is a plot of diffusivity versus resistivity for Al films with thickness less than 25 nm. The dashed line is the prediction from free-electron-gas theory.[26–32] Also included are diffusivity measurements on films co-deposited with the HEBs reported here. The potential thus exists for a short HEB mixer to have a -3 dB IF bandwidth of many tens of GHz if $L = 0.1$ μm can be utilized. We will show, however, that there is a lower limit on microbridge length, and thus a fundamental limit on

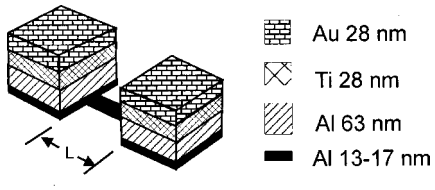

FIG. 2. Device geometry.

the maximum bandwidth achievable with a HEB with normal metal contact pads. For Al, the IF bandwidth is limited to about 8 GHz, which is still of great practical interest in many applications.

Although HEB mixers are intended for use at terahertz frequencies, the results presented here are for mixing measurements made with a 30 GHz microwave local oscillator. The motivation for these studies is to conduct a systematic set of measurements that would help understand the device physics relevant to the optimization of actual THz receivers. A similar approach was used successfully in the study of diffusion-cooled Nb HEBs.[21] We present mixing data for Al HEB mixers consisting of IF bandwidth, conversion efficiency, and noise measurements. Also, limitations on detector performance such as the minimum HEB length and saturation effects are discussed.

II. EXPERIMENTAL SETUP

A. Devices

The superconducting Al microbridges are 0.1 μm wide and vary in length from 0.2 to 1.0 μm. The device geometry is illustrated in Fig. 2. The microbridge thickness is 13–17 nm. The contact pads are made of thicker Al contacted with Ti and Au. The respective thicknesses of these layers is 63/28/28 nm. Deposition of the microbridge and contact pads is carried out without breaking the vacuum by way of a double angle evaporation so as to avoid the formation of oxide barriers. The devices are passivated with SiO which has proven helpful in maintaining long-term stability. Details of device fabrication can be found in Ref. 33.

The critical temperature of the microbridge varies from 1.4 to 2.5 K depending on resistivity. Devices with higher resistivity have a higher critical temperature, as is typical of thin Al films. The contact pads consist of layers of superconducting and normal metals, and have a superconducting transition at about 0.6 K. We chose to contact the microbridge with thicker Al rather than a normal metal film of Au or Pt directly to avoid the diffusion of the contact pad material into the microbridge. A perpendicular magnetic field $H = 0.05-0.12$ T is used to put the contact pads in the normal state, thus making the device ''N–S–N'' like conventional HEB mixers. The critical field of the contacts is significantly smaller than that of the microbridge, and thus it is possible to suppress superconductivity in the contacts while the T_C of the microbridge is only slightly reduced. The ability to switch between normal and superconducting contact pads has proven useful in understanding phenomena arising from the normal-superconductor proximity effect described later. In total, 14 Al HEBs were measured and the performance summary of some selected devices is given in Table I.

B. Measurement technique

Mixer measurements are made in a variable temperature liquid ^{3}He cryostat with a base temperature of 0.22 K. The LO source is a YIG oscillator (26.5–40 GHz) and the signal source is the internal generator of a HP 8722D network analyzer. The first IF amplifier is a high electron mobility transistor (HEMT) amplifier immersed in liquid ^{4}He. An isolator is used for narrow band noise measurements. The noise temperature and gain of the IF system is calibrated by measuring the Johnson noise of the device at zero-bias voltage as a function of bath temperature above T_C. The device output noise is typically measured in a ~50 MHz wide band between 1–2 GHz using a room temperature Schottky diode detector. This measurement system provides an environment with very low background radiation, with negligible leakage of room-temperature radiation. The device ''sees'' only cold terminations at 4 K. The effect of background radiation is of interest, and has proven in our work to be significant. In order to simulate thermal background noise which accompanies actual astronomical signals, the output from a broadband noise source is coupled in along with the rf signal using a broadband −3 dB combiner/divider. These measurements are useful in characterizing how susceptible the detector is to possible saturation effects. The mixer results reported here

TABLE I. Al HEB mixer parameters; measured in a perpendicular magnetic field, except devices C and H which are measured at a bath temperature $T > T_{C,\text{contacts}}$ and $H=0$. The microbridge width is 0.1 μm. The conversion efficiency and output noise given here are measured at IF=1 GHz.

Device	L (μm)	R_N (Ω)	T_{bath} (K)	IF BW (GHz)	η (dB)	T_{out} (K)	$T_M = T_{\text{out}}/2\eta$ (K,DSB)
A	0.2[a]	58	0.25	⋯	⋯	⋯	⋯
B	0.3[a]	33	0.22	⋯	⋯	⋯	⋯
C	0.3[b]	145	1.2	6	−27	⋯	⋯
D	0.6	48	0.22	⋯	−11	4	25
E	0.6	52	0.25	4	−8	1.3	4
F	0.6[c]	387	0.25	2	−16	1.6	32
G	1.0	100	0.22	⋯	−12	13.3	105
H	1.0[b]	260	1.2	1.2	−33	⋯	⋯

[a]Denotes a device without a superconducting transition.
[b]Poor conversion efficiency is observed since the bath temperature is close to T_C. A magnet was not present in the system at the time of these measurements.
[c]Poor conversion efficiency is observed because of the impedance mismatch between the device and the 50 Ω input impedance of the IF amplifier.

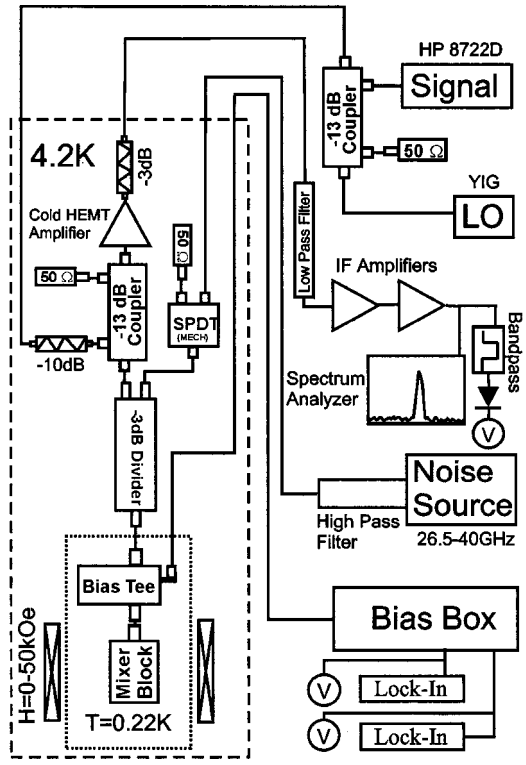

FIG. 3. Schematic of the measurement setup. The low pass filter cuts off at 12 GHz. The high pass filter consists of a pair of mated K_a band waveguide-coax adapters with a lower frequency cutoff of 26.5 GHz.

were measured without the extra noise source, except where it is explicitly stated otherwise. A schematic of the measurement setup is shown in Fig. 3. The various couplers and attenuators are included to ensure that the device sees only the LO and rf signal with only minimal additional noise from broadband room temperature noise, cables, amplifier, and other undesired sources, and that there are no unintentional microwave resonances in the cable assembly. We have checked carefully to confirm that these goals have been achieved.

III. RESULTS

A. dc properties

The resistance versus temperature characteristics in an applied magnetic field are shown in Fig. 4. The curves are

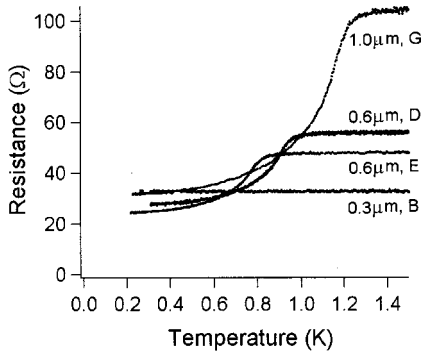

FIG. 4. Resistance vs temperature curves for devices G, D, E, and B, in a magnetic field; the contacts are nonsuperconducting. The microbridges have similar sheet resistance, $R_{sq}=R(W/L)$.

for four devices with very similar sheet resistance (R_{sq}) with lengths $L=0.3-1.0$ μm. The contact pads are in the normal state due to the magnetic field, and a sizable resistance is measured at temperatures significantly below the superconducting transition temperature of the microbridge. Without a magnetic field applied, two resistance drops are clearly visible (data not shown in Fig. 4); one for the microbridge at higher critical temperature and one for the contacts at lower critical temperature, at $\sim$0.6 K. The entire structure is superconducting at $T<0.6$ K and $H=0$. The measured resistance is that of the external wires, a few ohms. The maximum resistance of the two contact pads is estimated to be ~ 2 Ω. We therefore attribute the resistance below 0.6 K in a magnetic field to the suppression of superconductivity in the ends of the microbridge due to proximity effect from the normal metal contacts. This ~ 30 Ω resistance seen in Fig. 4 below $\sim$0.6 K can not be due to the resistance of the contact films. From measurements of the upper critical field (H_{c2}) of the microbridge the zero-temperature coherence length ξ is determined.[34] For the samples whose data is shown in Fig. 4 we have $\xi\sim 45$ nm, which agrees well with the relation $\xi = 0.855(\xi_0 l)^{1/2}$ if the resistivity is used to estimate the elastic mean free path l. Consider device G in Fig. 4 with $L=1.0$ μm with $R_N=100$ Ω. The residual resistance at low temperature (32 Ω) is likely due to two regions, one at each end of the microbridge, each of resistance 16 Ω. If this end region is assumed to be fully normal, its length would be 160 nm. This length, L_N, corresponds to $\sim 3.5\,\xi$. Thus, $(2L_N/L)*R_N$ is the total low temperature resistance. In samples with higher resistivity, the length of each resistive end scales at $L_N \sim 1/(T_C\rho)^{1/2}$ as does the coherence length. For example, sample E and sample F are both 0.6 μm long. These bridges (of different thickness) differ in resistivity by a factor of 5. The lengths of the resistive edge are $L_N=150$ nm for the clean device, sample E, and $L_N=70$ nm for the high resistivity device, sample F. For devices shorter than $6-7\xi$, such as device B in Fig. 4, no superconducting transition is observed. In this case, we believe that the entire microbridge is proximitized to be normal by the contact pads.

Several experiments were done to ensure that the observed low temperature resistance is not the result of external noise coupled to the devices. The presence of such noise could in principle suppress superconductivity in the weakest parts of the microbridge. R versus T measurements were made at Yale with and without microwave components in place and no differences were observed. Also, measurements were made in four different measurement systems (two at Yale University and two at the Jet Propulsion Laboratory) and similar results were obtained. It is believed that the applied field does not have any relation to this observed resistance, aside from the obvious effect of putting the contacts in the normal state. A *batch* of devices was fabricated with normal metal contacts (i.e., without thick Al) consisting of 28 nm of Ti and 70 nm of Au. The thin Al pads underneath the thick contact pads are proximitized normal by the thick Ti and Au layers above. These normal metal contact devices were unintentionally damaged prior to rf testing, and only dc measurements were conducted. The resistive transitions of the normal metal devices show the same residual resistance

at $T \ll T_C$ as the devices shown in Fig. 4 where a magnetic field is used to put the contacts into the normal state. The ends of the microbridge are forced into the normal state by proximity to the contacts regardless of whether the contacts are made normal through the application of a magnetic field or through the use of normal metal films. Thus, the arguments related to the effect of normal microbridge edges on mixer performance given below apply generally to N–S–N HEBs.

Measurements of the excess resistance in N–S–N structures have typically been for relatively large layered structures rather than narrow wires with thick contacts.[35,36] We have previously suggested[37] that the measured low temperature resistance can be predicted by applying the Usadel equations to calculate the position dependent superconducting energy gap for this geometry. Earlier predictions of the minimum length required to achieve a N–S–N structure have been made using Ginzburg–Landau theory.[38] Recently, work has been done at Delft University to explain the resistive transition in Al HEB structures within the Usadel framework. Initial simulations based on the Schmid–Schon approach indicate a good fit to the experimental data.[39]

There are various implications of this device residual resistance for HEB mixer performance. One main consequence relates to the maximum possible mixer IF bandwidth. We can define the minimum HEB length to be a multiple of the coherence length, $L_{\mathrm{Min}} = \beta\xi$. Substituting this into Eq. (3) and Eq. (2), the minimum thermal relaxation time and maximum IF bandwidth ($B_{\mathrm{IF,Max}}$) are determined. Since the diffusivity can be expressed as $v_F l/3$ with v_F the Fermi velocity, $B_{\mathrm{IF,Max}}$ depends only on the superconducting energy gap $\Delta(0)$, and is given by

$$B_{\mathrm{IF,Max}} \approx \pi^3 \Delta(0)/(2\beta^2 h), \tag{5}$$

where we use results for weak-coupling superconductors. This result is independent of other material specific parameters and should hold true for any HEB structures with fully normal contacts. Our experiments show that the Al microbridges do not exhibit a superconducting transition above 0.22 K when $\beta < 6-7 = \beta_c$. Devices slightly longer than $\beta_c \xi$ are only weakly superconducting, and are therefore likely to exhibit poor conversion efficiency. In order to estimate the maximum IF bandwidth in Al HEB mixers, we assume that $\beta\xi = 10\xi$ is the minimum microbridge length that yields working devices. The measured IF bandwidth, which is described in the next section, is ~1.5 times larger than that predicted by Eq. (3). Using the measured bandwidths as a scale correction to Eq. (3), we can derive the relationship

$$B_{\mathrm{IF,Max}} \approx (8 \ \ \mathrm{GHz}) \times T_C \tag{6}$$

for Al HEBs with normal contacts. Although this is sufficient IF bandwidth for most actual applications, it does constitute a limit which had previously not been considered. It should be noted that in Nb HEBs ξ is very small (~5 nm) and also that the areas underneath the contact pads are usually superconducting.[40] The combination of small coherence length and interface transparency is such that the thick normal metal contacts do not fully proximitize the thin Nb pads adjacent to the microbridge, and thus those areas adjacent to the microbridge are weakly superconducting. As a result, the suppression of superconductivity in the ends of the Nb microbridges is less significant. In any case, even with fully normal contacts, the predicted limits on IF bandwidth for Nb and Ta HEBs devices is a few tens of GHz, large enough for most applications.

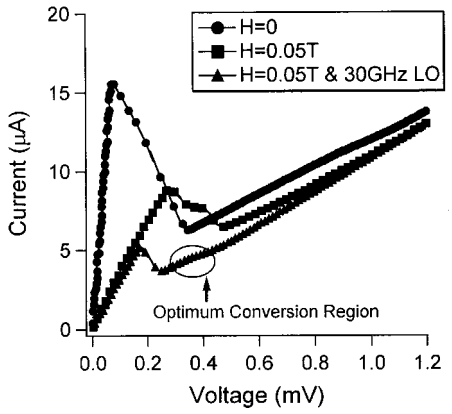

FIG. 5. Current–voltage curves of device G at $T = 0.22$ K.

In Al devices, the normal regions at the ends of the microbridge are evident in the current–voltage characteristics, shown in Fig. 5. The first two curves shown are the current–voltage characteristics with and without a magnetic field applied and no LO power applied. The resistance of a few ohms at low voltage in the $H = 0$ curve is due to the wiring. The resistance at low voltages in the presence of a magnetic field, about 30 ohms, is primarily due to the edges of the device being normal. The third curve shown is the LO pumped current–voltage characteristic in an applied magnetic field. The edge resistance gives rise to two possible regions of bias voltage where mixing is observed. Consider this curve, with LO power applied. Biasing below the first "kink" in the current–voltage characteristic, at voltages $V \leqslant 175$ μV, gives mixing response due to thermal modulation of the resistance in the two end regions of the device. Biasing above the second kink at voltages $V \geqslant 250$ μV, is also possible. Here, a large fraction of the device is resistive. It is in this large voltage region indicated by the circle in Fig. 5 where the best mixing is observed at microwave frequencies, as discussed next. This is also the region in which Nb HEBs are typically biased.

B. Intermediate frequency bandwidth

The -3 dB IF bandwidth is measured by sweeping the rf signal frequency, f_{rf}, while keeping the local oscillator frequency fixed and observing the amplitude of the IF signal. The IF power is fit to the form given in Eq. (1). The rf source is swept both above and below the LO frequency to ensure that resonances do not effect the bandwidth measurement. The coupling to the mixer at each rf frequency is estimated by measuring the power necessary to suppress the critical current of the microbridge to half its maximum value, with $P_{\mathrm{LO}} = 0$. A much smaller rf power than that required to suppress the critical current is used in the bandwidth measure-

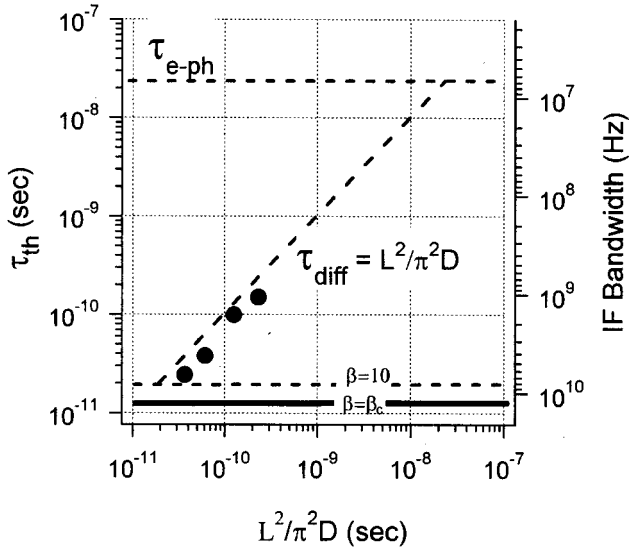

FIG. 6. Measured IF bandwidth vs diffusion-cooling prediction. The data correspond to devices H, F, E, and C in order of increasing IF bandwidth. The dotted $\beta=10$ line is an estimate of the maximum IF bandwidth of a sensitive, $T_C=1$ K HEB with normal contacts. Devices with a calculated IF bandwidth equal to or greater than that indicated by the solid black $\beta=\beta_c$ line do not exhibit a superconducting transition.

ment, and is adjusted at each frequency to deliver equal rf power to the mixer. This method was preferred to sweeping the LO source since the conversion efficiency varies with bias voltage changes ~ 10 μV. In our setup, the LO power can be adjusted in 1 dB increments, and it is difficult to ensure identical bias points for different LO frequencies. Both techniques did, however, yield similar results. The measured IF bandwidth ($f_{\mathrm{IF},-3\ \mathrm{dB}}$) is bias dependent. When the bias voltages is increased by ~ 50 μV or more from the optimum conversion point, the mixer conversion efficiency decreases strongly and the IF bandwidth increases by almost a factor of 1.5. The highest conversion efficiency occurs at voltages just above the unstable negative-resistance region in the current–voltage characteristic (see Fig. 5). We measured the IF bandwidth of several Al HEB mixers when biased for optimum conversion efficiency, for example, at $V\sim 220$ μV on the pumped current–voltage curve in Fig. 5. The thermal response time, τ_{th}, is derived from Eq. (2) and the measured IF bandwidths; this is plotted as a function of the calculated diffusion time in Fig. 6. The diffusion constant is determined using measurements of the upper critical magnetic field.[26] We observe in Fig. 6 that the IF bandwidth is proportional to D/L^2, and is therefore well described by the diffusion-cooling model. The measured IF bandwidth is approximately 50% larger than predicted from the film resistivity and the Wiedemann–Franz relation. We note that the electron–phonon inelastic time is about two orders of magnitude larger than the measured thermal relaxation, and thus electron–phonon interaction does not contribute significantly to the cooling of hot electrons in the Al HEBs measured here. Short devices ($L<0.3$ μm) made from low resistivity films should, in principle, have IF bandwidths >10 GHz, but

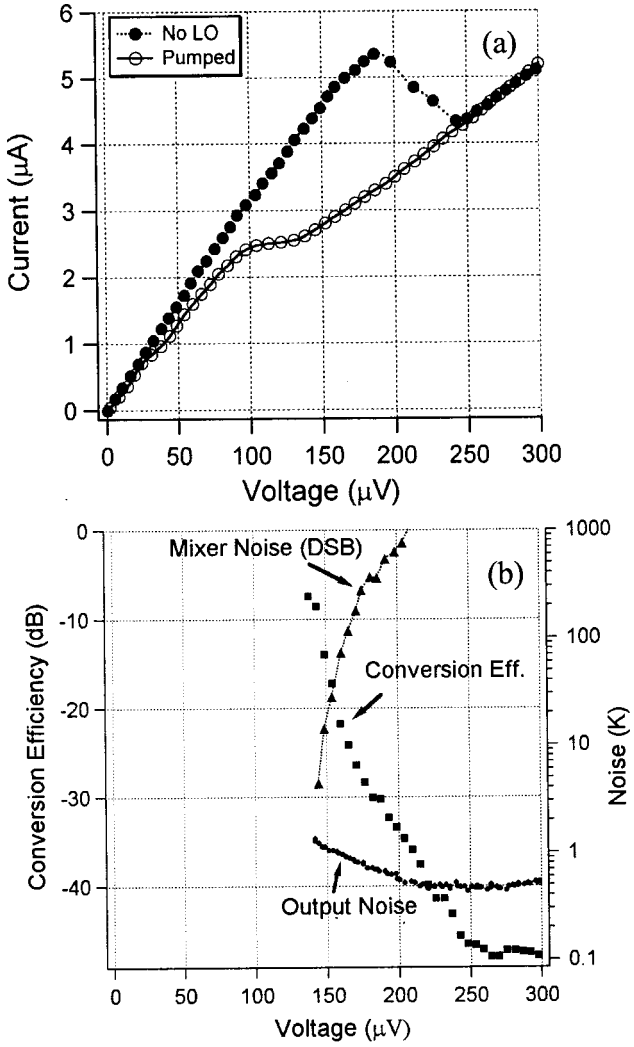

FIG. 7. The top figure (a) is the pumped current–voltage characteristic for device E. The bottom figure (b) is the corresponding mixer noise, output noise, and conversion efficiency vs bias voltage.

do not exhibit a superconducting transition in the microbridge when the contacts are in the normal state.

C. Mixer noise and conversion efficiency versus bias voltage

The conversion efficiency and mixer noise are shown for device E as a function of bias voltage in Fig. 7(b). The corresponding pumped current–voltage characteristic is plotted in Fig. 7(a). Data for areas of unstable operation are not shown. The optimum bias point for this device is at a lower voltage than that indicated for device G in Fig. 5 because both the critical current and T_C of device E are smaller. The double-sideband mixer noise temperature is inferred from the measured output noise temperature and single-sideband conversion efficiency η from $T_M=T_{\mathrm{out}}/2\eta$. The noise associated with the IF cables and cryogenic amplifier is subtracted from the output noise values shown in Fig. 7(b) and in Table I. By varying the bath temperature with the device in the normal state, it is possible to determine this IF chain noise and the overall IF gain. The best mixer noise temperature obtained is ~ 4 K for device E which has a 50 ohm normal resistance

that is well matched to our IF system. The data for T_M are for devices in an applied magnetic field. The difference in mixer noise between device E and device D is due to the fact that for device D the optimum magnetic field may not have been applied. We studied mixer performance with and without a magnetic field for devices 1.0 μm in length. Devices shorter than this displayed clear signs of Josephson mixing when the contacts were in the superconducting state. In this regime, peaks in the output noise are spaced $h\nu/2e$ apart in voltage and steps are seen in the pumped current–voltage characteristic. When biasing on these steps the conversion efficiency is near unity, the IF bandwidth is very large, and the output noise >100 K. For the 1 μm devices in which Josephson effects are not observed, without a magnetic field the output noise is ~ 20 K when operating at near optimum conversion efficiency. As the contacts are put in the normal state, the output noise decreases abruptly as a function of magnetic field and then levels off. If an applied magnetic field is too strong, superconductivity in the bridge is suppressed so much that the conversion efficiency is reduced more drastically than the output noise, which causes T_M to increase according to $T_M = T_{\text{out}}/2\eta$. For example, -8 dB conversion efficiency is also observed for device D but since a large enough magnetic field is not applied, the output noise is >10 K. The correlation between the state of the contacts, superconducting versus normal, and the device output noise is currently being studied. Devices E and D are indeed very similar in operation but with some observable differences arising from a more careful optimization procedure for the measurements on device E. In summary, device E shows the highest conversion efficiency and lowest mixer input noise. For devices D and E, where the mixer performance is good, the best results are obtained only within a narrow region of bias voltages, ~ 5–10 μV. The narrowness of this region makes these devices susceptible to output saturation effects if output noise voltages generated at the IF are a few μV or more, as discussed in Sec. III E.

D. Local oscillator power

The LO power used in the mixing experiments can be optimized for lowest noise performance or largest conversion efficiency. For a given power level, the mixer properties are measured as a function of bias voltage. The lowest noise or largest conversion attained is noted and then the LO power is incrementally changed. Typically the best noise performance is obtained by applying a LO power slightly greater (~ 1 dB) than that required for optimum conversion. In this slightly ''overpumped'' case, the output noise decreases by a few K from the optimum conversion case while the conversion efficiency decreases only slightly from its maximum value. In Fig. 8, we present the mixer noise and conversion efficiency as a function of LO power. An LO power within a few dB of the optimum value gives reasonably good performance. The magnitude and temperature dependence of the optimum LO power are shown in Fig. 9. For this set of measurements, the bath temperature is varied from $T = 0.25$ to 1.6 K. At each data point shown, the conversion efficiency versus bias voltage is measured for several different LO powers. The LO

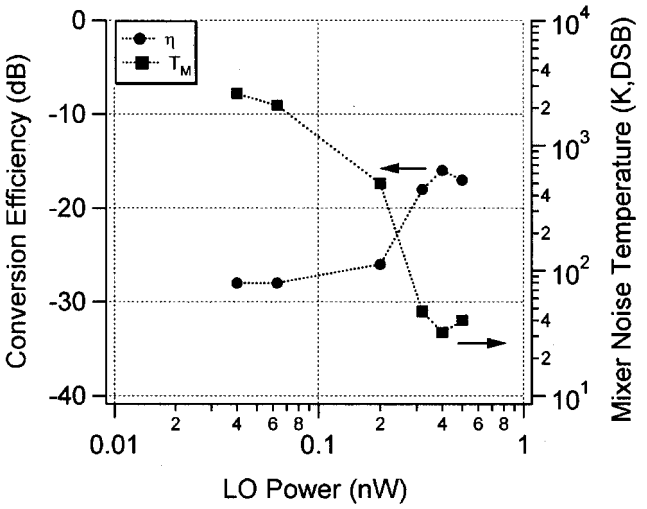

FIG. 8. Conversion efficiency and mixer noise as a function of LO power for device F.

power corresponding to the maximum conversion efficiency is reported in Fig. 9. These agree well with the prediction given in Eq. (4), shown as the dotted curve. At low temperatures, the optimum LO power for device F with normal state contacts is ~ 0.4 nW, as delivered to the mixer block, This is also approximately the power used in all the other mixing experiments described here.

E. Output saturation

Although good conversion efficiency, as large as -8 dB, is observed in the microwave measurements, the same results have not yet been obtained in the 618 GHz measurements.[41] The best conversion efficiency obtained there is ~ -20 dB. Also, the best conversion is measured in the ''lower'' voltage part of the current–voltage characteristic when mixing at 618 GHz. A possible explanation for this difference is output saturation of the device. Mixer saturation can occur both at

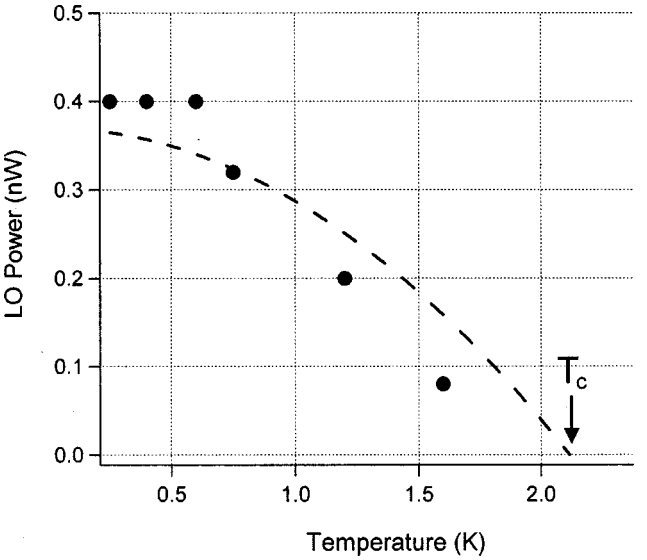

FIG. 9. LO power for optimum conversion efficiency vs bath temperature for Device F. The dashed line is the prediction from Eq. (4).

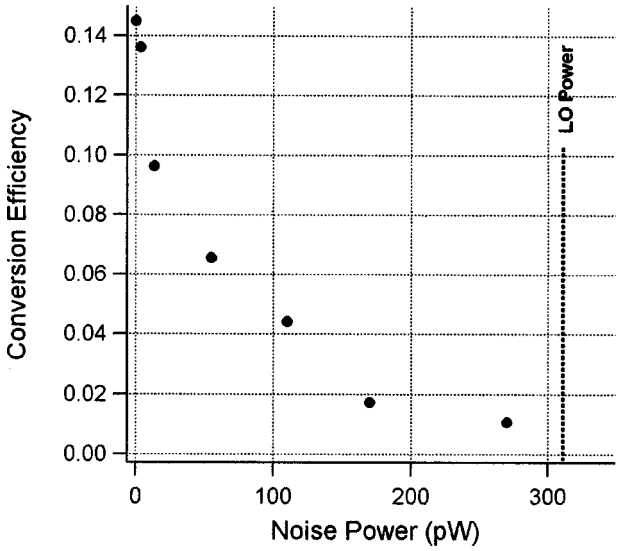

FIG. 10. Conversion efficiency vs incident input noise power for device D.

the input and at the output. We discuss output saturation first, as we believe that in the 618 GHz experiments it is the main mode of saturation. In our microwave data presented in Figs. 5–9, we believe that saturation effects do not occur, as we have taken care to have very low backgrounds. In any mixer, background thermal noise that couples to the mixer is down converted in frequency and creates a noise voltage at the IF. The relevant input noise bandwidth for this is twice the device IF bandwidth. If this noise voltage is large, it can cause an averaging or smearing of the dc current–voltage characteristic, and hence poor conversion efficiency. In the 30 GHz measurements, Fig. 7, we see that shifting the bias voltage from the optimum operating point by 10 μV causes the conversion efficiency to decrease by several dB. Consider as an example a 50 Ω device with an IF bandwidth of 4 GHz, conversion efficiency of -10 dB, and incident background radiation temperature of 100 K; this is an rf power of $kTB = 11$ pW. A peak-to-peak voltage of ~ 20 μV is thus generated at the IF. In our microwave experiments, the background noise is negligible due to the use of cryogenic attenuators. In the sub-mm wave experiments, quasioptical coupling is used and thermal noise from the room-temperature environment and warm optical losses is incident on the device. Both are much larger than at 30 GHz, possibly resulting in output saturation. To measure the effect of thermal background noise on mixer performance at 30 GHz, we combined the output of a noise source with the monochromatic rf signal. In Fig. 10, the conversion efficiency is shown as a function of noise power incident on the mixer block. The frequency of the incident noise is 26.5–36 GHz. The device used for the noise measurements has an IF bandwidth of 4 GHz and the LO frequency is 30 GHz. Thus, most of the incident noise is at a frequency that is down converted by the mixer. We can see a significant reduction in mixer conversion efficiency for noise powers only one tenth of P_{LO}, much smaller than the LO power. In contrast, when noise outside of the frequency band of down conversion is applied to the mixer, we see a significant degradation of conversion efficiency only when the applied noise power is 20% of the LO power. This is input saturation of the device, and is expected when the noise power is comparable to the LO power. Initial experiments at 618 GHz have been conducted in which cold quasioptical attenuators are used to reduce the background radiation. No significant improvement in conversion efficiency has so far been observed. Further work is necessary and will be discussed in a subsequent publication.[42]

IV. CONCLUSIONS

In microwave mixing experiments, Al HEB mixers demonstrate enhanced performance over higher T_C devices, as predicted. The output noise temperature of Al devices is considerably lower than that of Nb and NbN mixers. Conversion efficiency up to -8 dB is observed in the 30 GHz measurements, yielding very low inferred mixer noise temperatures. The LO power required for optimum mixing is ~ 0.5 nW. It should thus be possible to couple these mixers with solid state LO sources with output power of <1 μW. The measured IF bandwidth of the Al HEB mixers is well described by diffusion cooling and is proportional to D/L^2.

Along with the improvements summarized herein, we observed performance limitations associated with using low T_C HEBs. In the Al HEBs studied, the voltage range over which near-optimum performance is observed is narrow, $\Delta V_{-3\ \mathrm{dB},\eta} \sim 10$ μV. As such, these devices are susceptible to output saturation. If down converted thermal background radiation generates tens of microvolts of noise at the IF, then the mixer performance is significantly degraded. In addition to output saturation, we observed a minimum length for the microbridges to be superconducting. Microbridges shorter than $6-7\xi$ did not undergo a superconducting transition down to 0.22 K when contacted with fully normal pads. Requiring the microbridge to be longer than $L = 6-7\xi$ sets an upper bound on the IF -3 dB conversion bandwidth which depends only the superconducting energy gap. For Al, we estimate that IF bandwidth is limited to ~ 8 GHz for high sensitivity mixers, which is adequate for practical receiver applications.

Al HEB mixers are thus very sensitive but saturate easily. They could potentially be used in fully cryogenic setups where thermal loading has been minimized and the highest sensitivity is desired.

ACKNOWLEDGMENTS

The authors thank Professor R. J. Schoelkopf for use of some equipment and Professor M. Devoret and Dr. B. S. Karasik for useful discussions. This research was supported by the NSF AST 9618705 and the NASA Office of Space Science. Funding for one of the authors (I. S.) was provided by a NASA Graduate Student Fellowship.

[1] R. Blundell and C. E. Tong, Proc. IEEE **80**, 1702 (1992).
[2] G. J. Melnick, J. R. Stauffer, M. L. N. Ashby, E. A. Bergin, G. Chin, N. R. Erickson, P. F. Goldsmith, M. Harwit, J. E. Howe, S. C. Kleiner, D. G. Koch, D. A. Neufeld, B. M. Patten, R. Plume, R. Schieder, R. L. Snell, V. Tolls, Z. Wang, G. Winnewisser, and Y. F. Zhang, Astrophys. J. Lett. **539**, L77 (2000).
[3] J. W. Waters, W. G. Read, L. Froidevaux, P. F. Jarnot, R. E. Cofield, D. A.

Flower, G. K. Lau, H. M. Pickett, M. L. Santee, D. L. Wu, M. A. Boyles, J. R. Burke, R. R. Lay, M. S. Loo, N. J. Livesey, T. A. Lungu, G. L. Manney, L. L. Nakamuara, V. S. Perun, B. P. Ridenoure, Z. Shippony, P. H. Siegel, R. P. Thurstans, R. S. Harwood, H. C. Pumphrey, and M. J. Filipiak, J. Atmos. Sci. **56**, 194 (1999).
[4] T. G. Phillips and J. Keene, Proc. IEEE **80**, 1662 (1992).
[5] J. W. Waters, Proc. IEEE **80**, 1679 (1992).
[6] E. A. Bergin, G. J. Melnick, J. R. Stauffer, M. L. N. Ashby, G. Chin, N. R. Erickson, P. F. Goldsmith, M. Harwit, J. E. Howe, S. C. Kleiner, D. G. Koch, D. A. Neufeld, B. M. Pattern, R. Plume, R. Schieder, R. L. Snell, V. Tolls, Z. Wang, G. Winnewisser, and Y. F. Zhang, Astrophys. J. Lett. **539**, L129 (2000).
[7] M. C. Gaidis, H. M. Pickett, C. D. Smith, S. C. Martin, R. P. Smith, and P. H. Siegel, IEEE Trans. Microwave Theory Tech. **48**, 733 (2000).
[8] Proceedings of the ESA Symposium ''The Far Infrared and Submillimetre Universe'' (Grenoble, France, 15–17 April, 1997), p. 201.
[9] Proceedings of the IAU Symposium ''The Extragalactic Infrared Background and its Cosmological Implications,'' 15–18 August, 2000, Manchester, England.
[10] The National Research Council, *Federal Funding of Astronomical Research* (National Academy Press, Washington, DC, 2000).
[11] J. Kawamura, J. Chen, D. Miller, J. Kooi, J. Zmuidzinas, B. Bumble, H. G. LeDuc, and J. A. Stern, Appl. Phys. Lett. **75**, 4013 (1999); B. Jackson, G. de Lange, W. M. Laauwen, J. R. Gao, N. N. Iosad, and T. M. Klapwijk, *Proceedings of the 11th International Symposium on Space Terahertz Technology* (University of Michigan, Ann Arbor, MI, 2000), pp. 238–250.
[12] W. R. McGrath, *Proceedings of the International Symposium on Signals, Systems, and Electrons* (San Francisco, CA 1995), pp. 147–152.
[13] A. Skalare, W. R. McGrath, B. Bumble, H. G. LeDuc, P. J. Burke, A. A. Verheijen, and D. E. Prober, IEEE Trans. Appl. Supercond. **5**, 2236 (1995).
[14] B. S. Karasik, M. C. Gaidis, W. R. McGrath, B. Bumble, and H. G. LeDuc, Appl. Phys. Lett. **71**, 1567 (1997).
[15] J. C. Mather, Appl. Opt. **21**, 1125 (1982).
[16] E. M. Gershenzon, G. N. Gol'tsman, I. G. Gogidze, Y. P. Gusev, A. I. Elant'ev, B. S. Karasik, and A. D. Semenov, Superconductivity **3**, 1582 (1990).
[17] D. E. Prober, Appl. Phys. Lett. **62**, 2119 (1993).
[18] Yu. P. Gousev, G. N. Gol'tsman, A. D. Semenov, E. M. Gershenzon, R. S. Nebosis, M. A. Heusinger, and K. F. Renk, J. Appl. Phys. **75**, 3695 (1994).
[19] S. Cherednichenko, M. Kroug, P. Yagoubov, H. Merkel, E. Kollberg, K. S. Yngvesson, B. Voronov, and G. Gol'tsman, in *Proceedings of the 11th International Symposium on Space Terahertz Technology* edited by J. East (University of Michigan, Ann Arbor, MI, 2000), pp. 219–227.
[20] A. D. Semenov, H.-W. Hubers, J. Schubert, G. N. Gol'tsman, A. I. Elantiev, B. M. Voronov, and E. M. Gershenzon, J. Appl. Phys. **88**, 6758 (2000).
[21] P. J. Burke, R. J. Schoelkopf, D. E. Prober, A. Skalare, B. S. Karasik, M. C. Gaidis, W. R. McGrath, B. Bumble, and H. G. LeDuc, J. Appl. Phys. **85**, 1644 (1999).
[22] R. A. Wyss, B. S. Karasik, W. R. McGrath, B. Bumble, and H. LeDuc, in *Proceedings of the Tenth International Symposium on Space Terahertz Technology*, edited by T. Crowe and R. M. Weikle (University of Virginia, Charlottesville, VA, 1999), pp. 215–228.
[23] B. S. Karasik and W. R. McGrath, in *Proceedings of the Ninth International Symposium on Space Terahertz Technology*, edited by W. R. McGrath (Pasadena, CA, 1998), pp. 73–80.
[24] B. S. Karasik and A. I. Elantiev, Appl. Phys. Lett. **68**, 853 (1996).
[25] P. J. Burke, Ph.D. thesis, Yale University, 1997.
[26] J. M. Gordon and A. M. Goldman, Phys. Rev. B **34**, 1500 (1986).
[27] Y. Bruynserade, M. Gijs, C. Van Haesendonck, and G. Deutscher, Phys. Rev. Lett. **50**, 277 (1983).
[28] P. Santhanam and D. E. Prober, Phys. Rev. B **29**, 3733 (1984).
[29] B. Shinozaki, T. Kawaguti, and Y. Fujimori, J. Phys. Soc. Jpn. **61**, 3678 (1992).
[30] E. M. Gershenzon, G. N. Gol'tsman, V. D. Potapov, and A. V. Sergeev, Solid State Commun. **75**, 639 (1990).
[31] M. Park, K. R. Lane, J. M. Parpia, and M. S. Isaacson, J. Vac. Sci. Technol. A **13**, 127 (1995).
[32] C. Kittel, *Introduction to Solid State Physics* 7th ed. (Wiley, New York, 1996), p. 158; $v_F = 1.3 \times 10^6$ m/s to be consistent with Refs. 26–31.
[33] P. M. Echternach, H. G. LeDuc, A. Skalare, and W. R. McGrath, in *Proceedings of the Tenth International Symposium on Space Terahertz Technology*, edited by T. Crowe and R. M. Weikle (University of Virginia, Charlottesville, VA, 1999), pp. 261–268.
[34] M. Tinkham, *Introduction to Superconductivity* 2nd ed. (McGraw–Hill, New York, 1996), p. 162.
[35] Y. Krahenbuhl and R. J. Watts-Tobin, J. Low Temp. Phys. **35**, 5 (1979).
[36] C. C. Chi, P. Santhanam, S. J. Wind, M. J. Brady, and J. J. Bicchigano, Phys. Rev. B **50**, 3487 (1994).
[37] I. Siddiqi, A. Verevkin, D. E. Prober, A. Skalare, B. S. Karasik, W. R. McGrath, P. Echternach, and H. G. LeDuc, IEEE Trans. Appl. Supercond. **11**, 958 (2001).
[38] W. Liniger, J. Low Temp. Phys. **93**, 1 (1993).
[39] A. Verbruggen, T. M. Klapwijk, W. Belzig, and J. R. Gao, *Proceedings of the 12th International Symposium on Space Terahertz Technology* 14–16 February, 2001, San Diego, CA, pp. 42–46.
[40] D. Wilms Floet, J. J. A. Baselmans, and T. M. Klapwijk, Appl. Phys. Lett. **73**, 2826 (1998).
[41] A. Skalare, W. R. McGrath, P. M. Echternach, H. G. LeDuc, I. Siddiqi, A. Verevkin, and D. E. Prober, IEEE Trans. Appl. Supercond. **11**, 641 (2001).
[42] W. R. McGrath (unpublished).